Journal of Applied Physics ARTICLE pubs.aip.org/aip/jap

Photoluminescence identification of the V_{Si} and N_C–V_{Si} defects in 4H-SiC generated by keV Si ion irradiation

Cite as: J. Appl. Phys. **138**, 113102 (2025); doi: 10.1063/5.0278808
Submitted: 2 May 2025 · Accepted: 28 August 2025 ·
Published Online: 15 September 2025

Shyama Rath,[1,a] Gaurav Gupta,[1] and Shin-ichiro Sato[2]

AFFILIATIONS

[1]Department of Physics and Astrophysics, University of Delhi, Delhi 110007, India
[2]National Institutes for Quantum Science and Technology (QST), 1233 Watanuki, Takasaki, Gunma 370-1292, Japan

[a]**Author to whom correspondence should be addressed:** srath@physics.du.ac.in

ABSTRACT

The quantum properties of the silicon vacancy (V_{Si}) and nitrogen-vacancy complex (N_C–V_{Si}) defects in 4H-SiC are a subject of ongoing research due to applications in quantum metrologies. While MeV proton irradiation has been widely used for N_C–V_{Si} generation, the intermediate V_{Si}–H complex is detrimental. This study uses Si ions of keV energies conveniently achievable from a modest ion implanter to generate both V_{Si} and N_C–V_{Si}. Their signatures and densities are determined by photoluminescence (PL) spectroscopy and the intensities compare well with previous studies using MeV ions. Two types of 4H-SiC, high purity semi-insulating and n-type, are investigated. In the pristine semi-insulating sample, V_{Si} is already present, and the intensity increases with a fluence up to 1×10^{14} cm^{-2} and decreases thereafter for 1×10^{15} and 1×10^{16} cm^{-2}. A post-implantation thermal annealing further modulates the V_{Si} PL emission. On the other hand, in the pristine n-type wafer, the V_{Si} defect is absent due to its high dopant concentration, but is created after an implantation at a fluence of 1×10^{12} cm^{-2}. The N_C–V_{Si} defect in n-type is not activated even up to an ion fluence of 1×10^{16} cm^{-2} but emerges after a post-implantation annealing. Thus, a judicious choice of ion fluence and annealing controls the formation and the density of V_{Si} and its conversion to N_C–V_{Si} defects in SiC. Wavelength dependent photoluminescence spectroscopy gives further insights into the defects. The defect densities are correlated to the ion-induced structural disorder and thermally induced recrystallization monitored by Raman spectroscopy.

I. INTRODUCTION

Point defects in solid-state systems are being actively investigated for their viability as potential candidates for qubits relevant for emerging technologies, such as quantum information processing and metrology.[1,2] Among the contenders for qubits in solid-state systems, the nitrogen-vacancy center created by replacing a single carbon atom in a diamond's atomic lattice with a nitrogen atom and leaving a neighboring lattice site empty is a well-known example.[3–6] Inspired by the viability of this defect qubit in diamond, other material systems as hosts for similar point defects are being actively explored. Silicon carbide (SiC) is closely related to diamond in its electronic structure and is a viable host for a variety of point defects.[7,8] Some of these point defects are the single negatively charged silicon monovacancy (hereafter denoted as V_{Si}),[9–15] the carbon antisite–carbon vacancy pair (C_{Si}–V_C),[16,17] the neutral divacancy consisting of a carbon vacancy adjacent to a silicon vacancy (V_{Si}–V_C),[18,19] and vacancy–impurity complexes, such as the single negatively charged nitrogen-vacancy center in which the substitutional nitrogen in the carbon site sits next to a Si vacancy (N_C–V_{Si}).[20–24] In particular, the room temperature luminescence properties of V_{Si} and N_C–V_{Si} and their non-zero spins along with the mature and well-established crystal growth and device fabrication technologies of SiC contribute to their applications for quantum technologies.[25]

The V_{Si} defect in 4H-SiC has a C_{3v} symmetry and can form at two different sites, hexagonal (h) or quasi-cubic (k), and termed as V_1 and V_2, respectively. According to C_{3v} symmetry, the suspended bonds consist of two A_1-levels and one doubly degenerate E-level. The V_1 and V_2 centers emit at two distinct wavelengths of 861 (~1.44 eV) and 916 nm (~1.35 eV) corresponding to the transition

from the ^4E excited state to the $^4A_2$ ground state and from the excited $^4A_2$ to the ground $^4A_2$ state,[14] respectively. V_{Si} has been demonstrated to have a long room temperature spin coherence time (T_2 of ~100 μs) and a high spin (S = 3/2).[12–14]

The occurrence of the N_C–V_{Si} defects in 4H-SiC depend on the location of V_{Si} in the lattice.[20,21] The N atom is either on the *c*-axis or in the basal plane and the non-equivalent carbon sites have *h* or *k* adjacent symmetries. The structure contains four types of N_C–V_{Si} centers, including two axial (*kk* and *hh*) and two basal (*hk* and *kh*). The axial and the basal centers possess different symmetries, C_{3v} and C_{1h}, respectively, leading to emission at different wavelengths: 1173 nm (*kh*), 1179.9 nm (*hh*), 1223.5 nm (*kk*), and 1243.6 nm (*hk*).[20,24] Thus, all the emissions occur in the telecom wavelength region in contrast to the visible region (538 and 638 nm) emission of the N–V center in diamond. This room temperature emission in the near-infrared (NIR) region makes them relevant both for quantum communication and for biological application, such as *in vivo* imaging due to the greater penetration of near NIR wavelengths in tissues as compared to visible light.[26]

The promising properties of the V_{Si} and N_c–V_{Si} centers in SiC for quantum metrology calls for convenient protocols for their generation, detection, and enhancing their density. V_{Si} has been generated by irradiation using energetic particles, such as electrons,[11,27–29] neutrons,[30,31] protons,[32–36] and ions.[33,37,38] N_c–V_{Si} centers are commonly formed through the V_{Si} defects created by proton irradiation. These become mobile, diffuse, and pair with the nitrogen centers in n-type 4H-SiC by a subsequent annealing to form N_C–V_{Si}.[20–23,33–36] However, proton irradiation, in addition to forming the V_{Si} defects required for N_C–V_{Si} formation, also forms detrimental V_{Si}–H complexes which in turn hinder the formation of N_C–V_{Si}, and, therefore, H ion beams are not very desirable.[22,23,34–36] In a previous study, Sato *et al.*[33] explored other ions with MeV energies, such as 2 MeV nitrogen, 4 MeV silicon, and 7 MeV iodine in addition to proton irradiation to generate both V_{Si} and N_C–V_{Si} defects. A post-irradiation annealing quenched the V_{Si} emission but enhanced the N_C–V_{Si} center emission demonstrating that the fluence and annealing temperature determined the relative intensities of both the defects. The N_C–V_{Si} intensity was also found to be greater for the heavier ion. From a practical point of view, the use of keV rather than MeV energies would be desirable as they can be conveniently obtained using a relatively small, cost-effective accelerator (ion implanter).

This study aims to demonstrate the formation of the V_{Si} and N_C–V_{Si} defects with keV energies of self-ion implantation (i.e., Si in SiC). Self-ion implantation can create point defects without adding any impurity. While Si ions should normally result in a Si-rich condition, the implantation damage is significant enough to offset the effect of the Si-rich condition, which would otherwise enhance the formation energy of silicon vacancies. [Transport range of ions in matter (TRIM) calculations of V_{Si} and implanted Si are presented in the supplementary material.] Si ion implantation, thus, creates V_{Si} defects without forming the detrimental V_{Si}–H complexes seen with proton irradiation. Also, Si being heavier compared to H has a shallower implantation depth and could create a greater density of defects in the same volume. With this perspective, 200 keV Si ion of varying ion fluence and a post-implantation thermal annealing is used. Photoluminescence (PL) spectroscopy, which is rapid, contactless, and not requiring any sample preparation, is a useful metrology for the identification of these defects having optical signatures. The two types of wafers investigated, namely, high purity semi-insulating (HPSI) and n-type, demonstrate the effect of the dopant concentrations on the defect generation. In HPSI, where V_{Si} is already present in the pristine wafer, the ion fluence modulates its intensity. An increase of fluence from 1×10^{13} to 1×10^{14} ions/cm^2 results in an almost twofold increase in the PL intensity indicating an increase in the V_{Si} concentration. The intensity thereafter decreases for higher fluences of 1×10^{15} and 1×10^{16} cm^{-2} due to the disorder, but a subsequent annealing enhances the intensity. In n-type, V_{Si} is absent in the pristine wafer due to a high dopant concentration but is activated by implantation. A subsequent thermal annealing generates N_c–V_{Si} while the V_{Si} intensity decreases. The enhancement/quenching of the defect-related PL emission correlates with the ion-induced disorder/amorphization and thermally induced recrystallization as observed in the Raman spectra. The spin signature of V_{Si} in the HPSI wafer is observed in the optically detected magnetic resonance (ODMR) spectrum.

II. EXPERIMENTAL DETAILS

Two types of 4H-SiC single-crystal wafers, namely, high purity semi-insulating (HPSI) and n-type U200 procured from Cree, are used in this study. Silicon ion implantation of the HPSI and n-type U200 wafers was performed at Inter University Accelerator Center, India and at Takasaki Institute for Advanced Quantum Science,

TABLE I. Parameters of the HPSI and n-type U200 4H-SiC wafers.

	4H-SiC	
Parameters	High purity semi-insulating (HPSI)	n-type U200
Thickness	332.8 μm	350 μm
Average resistivity	1×10^9 Ω cm	0.015–0.028 Ω cm
Orientation	On-axis	4° off-axis
Doping density	…	5×10^{18}–1×10^{19} cm^{-3}
Face	Double sided polish Si face	Double sided polish Si face
Ion species and energy	200 keV Si ions	200 keV Si ions
Fluence	1×10^{13}, 1×10^{14}, 1×10^{15}, 1×10^{16} cm^{-2}	1×10^{12}, 1×10^{13}, 1×10^{14}, 1×10^{15}, 1×10^{16} cm^{-2}
Annealing temperature/time	800 °C/30 min	700 and 1000 °C/30 min

Japan, respectively. The implantations were performed at room temperature and the sample surface was not covered. Subsequently, the samples were thermally annealed under an Ar atmosphere. The sample details along with the implantation fluences and annealing conditions are mentioned in Table I. The annealing conditions (range of temperatures and time) were selected based on previous reports. Since no intercomparison between the HPSI and n-type wafers is being made, the differences in their annealing temperatures do not affect the results. V_{Si} formed by the implantation could transform into either divacancies or antisite-vacancy pairs for annealing temperatures above 1000 °C, and, therefore, the temperature has been restricted to 1000 °C.

The room temperature PL spectra were recorded using a Horiba LabRAM HR evolution system (the micro-PL/Raman measurement system). Three excitation wavelengths of 532, 785, and 1064 nm were used to span the wide spectral range of the defects. The PL signals were detected using a CCD detector for the 532 nm excitation wavelength and an InGaAs detector for the 785 and 1064 nm excitation wavelengths. The data were collected with an objective lens (numerical aperture (NA) is 0.90 for 100× for the visible range and 0.80 for 50× for the NIR range at RT).

III. RESULTS AND DISCUSSION

A. Comparison between pristine HPSI and n-type U200 wafers

1. Photoluminescence spectra

The comparative PL spectra of the pristine HPSI and n-type U200 samples measured using a 532 nm excitation are depicted in Fig. 1. The spectrum of the HPSI wafer clearly shows the presence of V_{Si} through a broad peak ranging between 850 and 1000 nm and centered at around 916 nm.[11,33,34,36,37] In comparison, no significant emission is observed in the n-type U200 pristine wafer around this wavelength region, indicating an absence of V_{Si} defects. This is due to the high dopant concentration in the n-type wafers. Compared to the HPSI wafers, the n-type SiC wafer with a high concentration of nitrogen doping may have its Fermi level shifted closer to the conduction band edge, which may change the charge state of the V_{Si} defect and introduce new competitive pathways, such as non-radiative recombination centers, quenching the V_{Si} peak in the PL spectrum. The abundant electrons due to the high doping in the n-type fill the defect levels and impact the capture of carriers by these defect states. Thus, the negatively charged V_{Si} may no longer be the dominant charge state.[15,31,38] The negatively charged V_{Si} state has been demonstrated to be stable in HPSI. However, it can only be stable in n-type if its concentration is larger than that of the donor concentration.[31] It is, therefore, absent in the n-type U200 wafers which have a high concentration of donors of the order of 5×10^{18}–1×10^{19} cm^{-3}. V_{Si} in charge states other than the negatively charge one do not have an optical signature and, therefore, not detected through PL spectroscopy. This difference in the V_{Si} intensity is a key feature of the pristine HPSI and n-type wafers having different dopant concentrations. The broad peak centered at 680 nm observed in both wafers, albeit with different intensities relative to V_{si}, is attributed to the C_{Si}–V_C defect.[16,17]

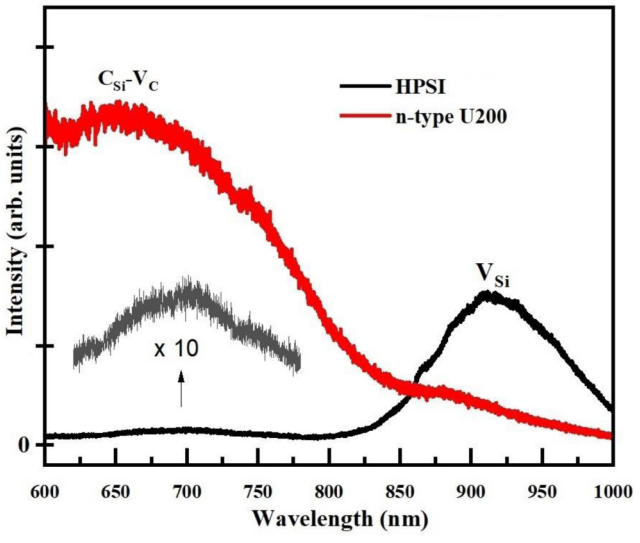

FIG. 1. Room temperature PL spectra of the pristine HPSI and n-type U200 wafers.

2. Raman spectra

The comparative Raman spectra of the HPSI and n-type U200 pristine samples measured using a 532 nm excitation wavelength are depicted in Fig. 2. The observed phonon modes and the assignments are E_2 (TA: transverse acoustic) mode at 204 cm^{-1}, A_1 (LA: longitudinal acoustic) mode at 610 cm^{-1}, E_2 (TO: transverse optical) mode at 776 cm^{-1}, E_1(TO) mode at 797 cm^{-1}, and A_1 (LO: longitudinal optical) at 964 $cm^{-1}$and are identifiable from previous studies.[39–41] A key difference between the two wafers is in the

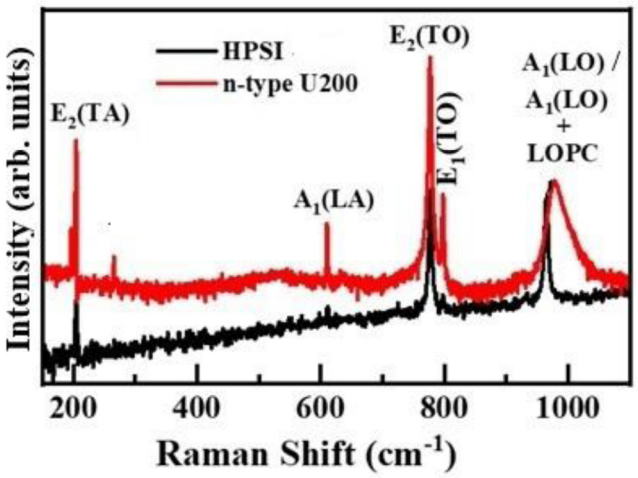

FIG. 2. First-order Raman spectra of the pristine HPSI and n-type U200 wafers.

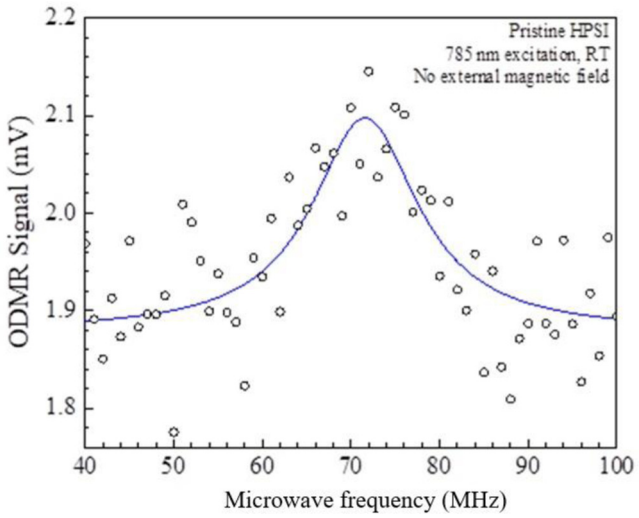

FIG. 3. Room temperature ODMR spectrum of V_{Si} in the pristine HPSI wafer without an external magnetic field (open symbols). The experimental data were fitted by a Lorentzian function (blue line).

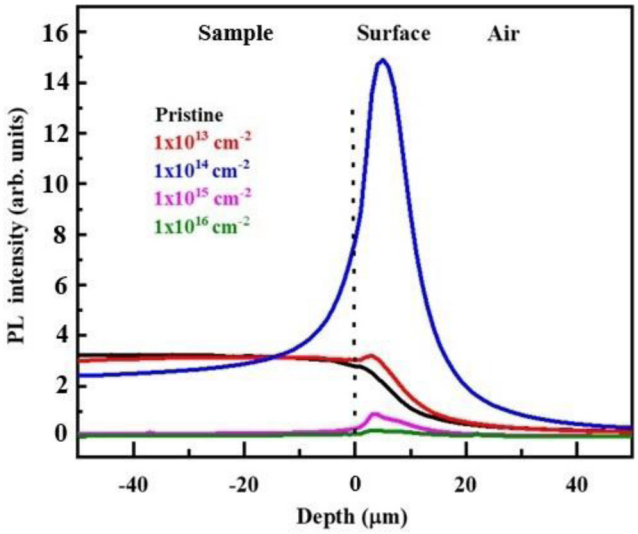

FIG. 4. PL intensity of the V_{Si} emission as a function of the distance between the focal point and the sample surface of irradiated 4H-SiC.

lineshapes of the phonon mode between 925 and 1100 cm^{-1} (LO). While a sharp A1 (LO) mode is observed at 964 cm^{-1} for the HPSI wafer, the n-type U200 wafer exhibits a broad asymmetric peak between 930 and 1100 cm^{-1}. This originates from the interaction of collective excitation of free carriers (from the large dopant concentration) with LO phonons via their macroscopic electric fields in polar semiconductors. The peak is a combination of the A_1 (LO) and longitudinal-optic plasmon coupled (LOPC) modes.

3. ODMR spectrum of V_{Si} in the HPSI wafer

The optically detected magnetic resonance (ODMR) spectrum of the V_{Si} defect present in the pristine HPSI wafer is depicted in Fig. 3. In this measurement, the pristine HPSI wafer was placed on a coplanar waveguide, and the change in photon emission intensity of V_{Si} was investigated when the microwave was applied to the waveguide. The excitation wavelength was 785 nm, and a 900 nm longpass filter was placed in front of a photodiode to only collect

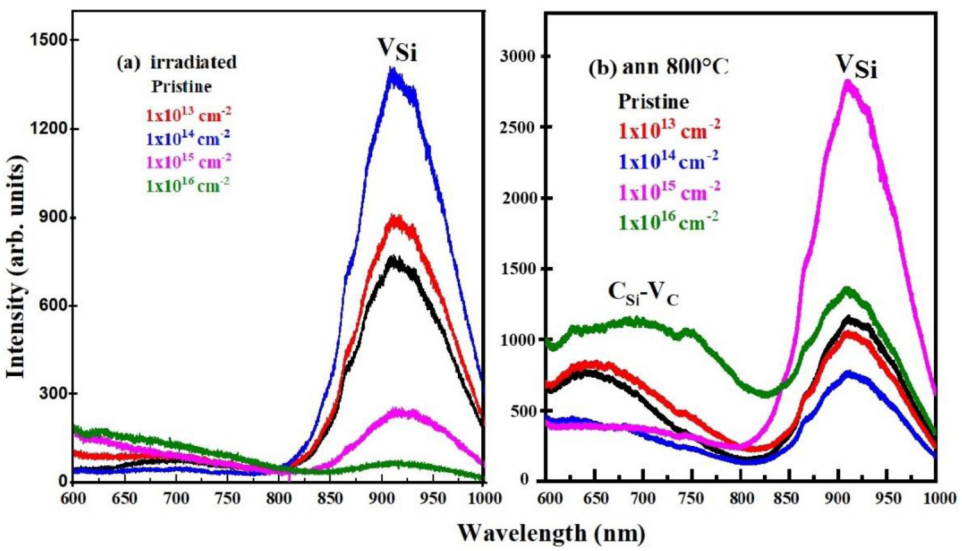

FIG. 5. Room temperature PL spectra of (a) as-implanted and (b) annealed HPSI wafers excited using a 532 nm laser.

the photon emission of V_{Si} defects at the *k* site. The change in photodiode output due to the magnetic resonance was detected using a conventional lock-in detection technique (AM modulation). Since no external magnetic field was applied, a resonance peak due to the zero-field splitting of the ground level was observed at around 70 MHz. The appearance of the peak at 70 MHz provides further evidence that the broad emission peak at 800–1000 nm observed in the PL spectrum is due to the photon emission of V_{Si} defects.[42]

B. Photoluminescence study of the ion-irradiated and thermally annealed HPSI wafers

Confocal microscopy is used for a depth-profiling of the V_{Si} emission centered at 916 nm. Figure 4 shows the intensity profile of the V_{Si} peak as a function of the distance between the focal point of the objective and the sample surface taken using an excitation of 785 nm. The depth value of +3 to +5 μm describes the sample surface, and the positive and negative depth values describe the distances when the focal point is above the sample surface (air) and in the sample, respectively. The intensity profile of the PL peak shows a maximum close to the surface since the penetration depth of the 200 keV Si ion in SiC is only around 300 nm. The intensity increases for a fluence of 1×10^{14} cm^{-2} and thereafter decreases for 1×10^{15} and 1×10^{16} cm^{-2} due to the amorphization as evidenced by Raman measurements.[43]

The room temperature PL spectra of the irradiated HPSI wafers recorded using an excitation wavelength of 532 nm is depicted in Fig. 5(a). With an increase of the ion fluence from 1×10^{13} to 1×10^{14} cm^{-2}, there is an almost twofold increase in the V_{Si} PL intensity which is indicative of an increase in the concentration of V_{Si}. The intensity thereafter decreases for the higher fluences of 1×10^{15} cm^{-2} and 1×10^{16} cm^{-2} due to the non-radiative channels introduced by the disorder at higher fluences. After annealing, the PL intensity improves substantially for both these fluences as seen in Fig. 5(b) because of the recovery of the ion-induced disorder after annealing. The P signatures of the V_{Si} concentration with irradiation and annealing correlate with the disorder/amorphization and recrystallization reported using Raman spectroscopy, Rutherford backscattering, and high-resolution x-ray diffraction in our earlier study.[44] The hump observed in the range between 600 and 700 nm after annealing has been reported as the C_{Si}–V_C defect.[16,17]

C. Photoluminescence spectra of the ion-irradiated and thermally annealed n-type U200 wafers

1. Effect of ion irradiation

The PL spectra of the as-implanted n-type U200 wafers excited at different wavelengths are shown in Figs. 6(a)–6(c). The use of different wavelengths allows us to span a wide spectral range. The V_{Si} emission, absent in the pristine sample, emerges after Si implantation. The intensity increases with implantation from 1×10^{12} to 1×10^{14} cm^{-2} and decreases thereafter for fluences of 1×10^{15} and 1×10^{16} cm^{-2}. The trend of the V_{Si} PL emission with fluence is similar to that of the HPSI samples and correlates to the disorder and amorphization as observed in the Raman spectra described below for the n-type wafers. The same trend is observed for measurements made with both 532 and 785 nm excitations [Figs. 6(a) and 6(b)]. It is pertinent to mention that the PL intensities will depend on the laser wavelength. A greater proximity to an energy level activates the emission more effectively, in this case 785 nm to the V_{Si} level. We have observed this intensity difference in the V_{Si} PL emission in HPSI wafer for measurements made with 532 and 785 nm (Fig. 2 of the supplementary material). The

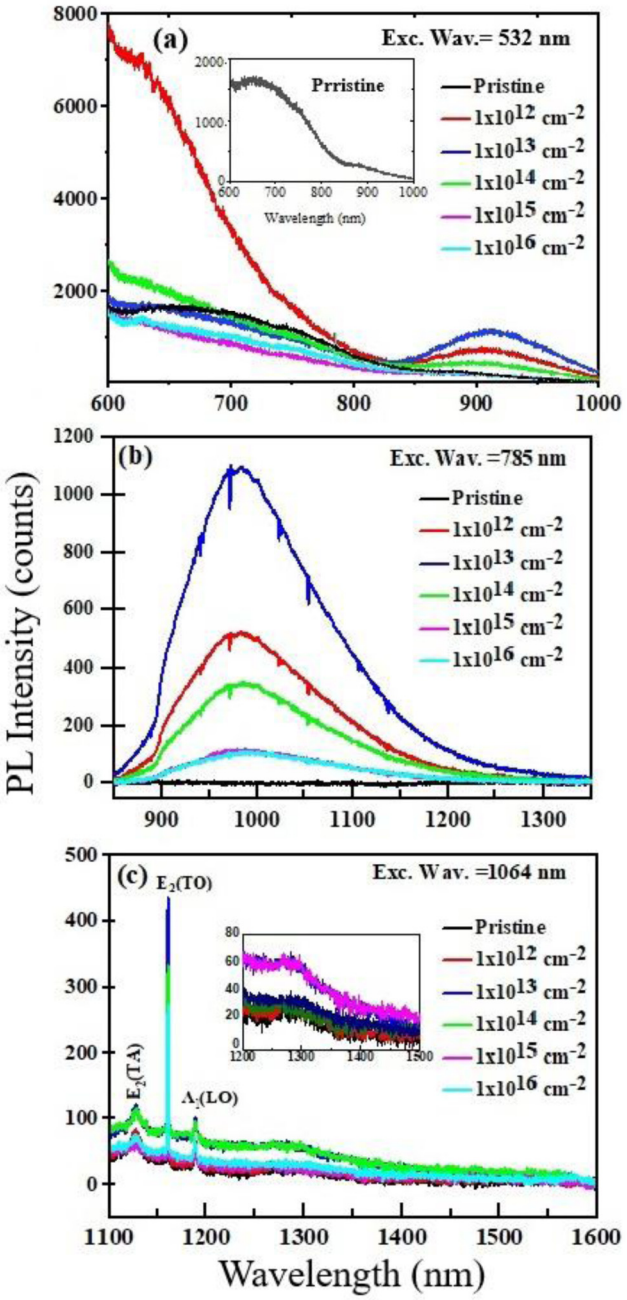

FIG. 6. Room temperature PL spectra of as-implanted n-type U200 excited using (a) 532, (b) 785, and (c) 1064 nm wavelengths.

V_{Si} PL has been reported to be less efficient for wavelengths less than 760 nm, with 770 nm being the optimum wavelength determined through photoluminescence excitation spectroscopy.[44] For the 1064 nm excitation, the broad peak observed at 1290 nm is presumably due to the N_C–V_{Si} centers [Fig. 6(c)].[33–36] The sharp peaks at around 1127, 1159, and 1188 nm are the E_2 (TA), E_2 (TO), and A_1 (LO) Raman modes, respectively, as explained earlier in the manuscript.

2. Effect of thermal annealing

a. For an excitation wavelength of 785 nm. The comparative PL spectra for the pristine, irradiated, and annealed n-type U200 wafers are depicted in Figs. 7(a)–7(f). The annealing was done at two temperatures of 700 and 1000 °C for 30 min. The V_{Si} defect is completely absent in the pristine sample due to the higher n-dopant concentration as explained earlier and is not significantly changed after annealing [Fig. 7(a)]. V_{Si} emerges only after an irradiation, with the highest intensity occurring for a fluence of 1×10^{13} cm^{-2}. An annealing thereafter is seen to modulate the V_{Si} PL intensity. It is suppressed after annealing of the 1×10^{12} cm^{-2} irradiated wafer. For the higher fluence of 1×10^{13} cm^{-2}, the intensity decreases by a factor of half after annealing at 700 °C and thereafter becomes negligible for 1000 °C. For 1×10^{14} cm^{-2}, there is no significant change in V_{Si} after annealing at 700 °C, but gets suppressed for 1000 °C. An annealing of the 1×10^{15} and 1×10^{16} cm^{-2} irradiated wafers at 1000 °C suppresses V_{si} and instead a sharper peak emerges at around 900 nm.

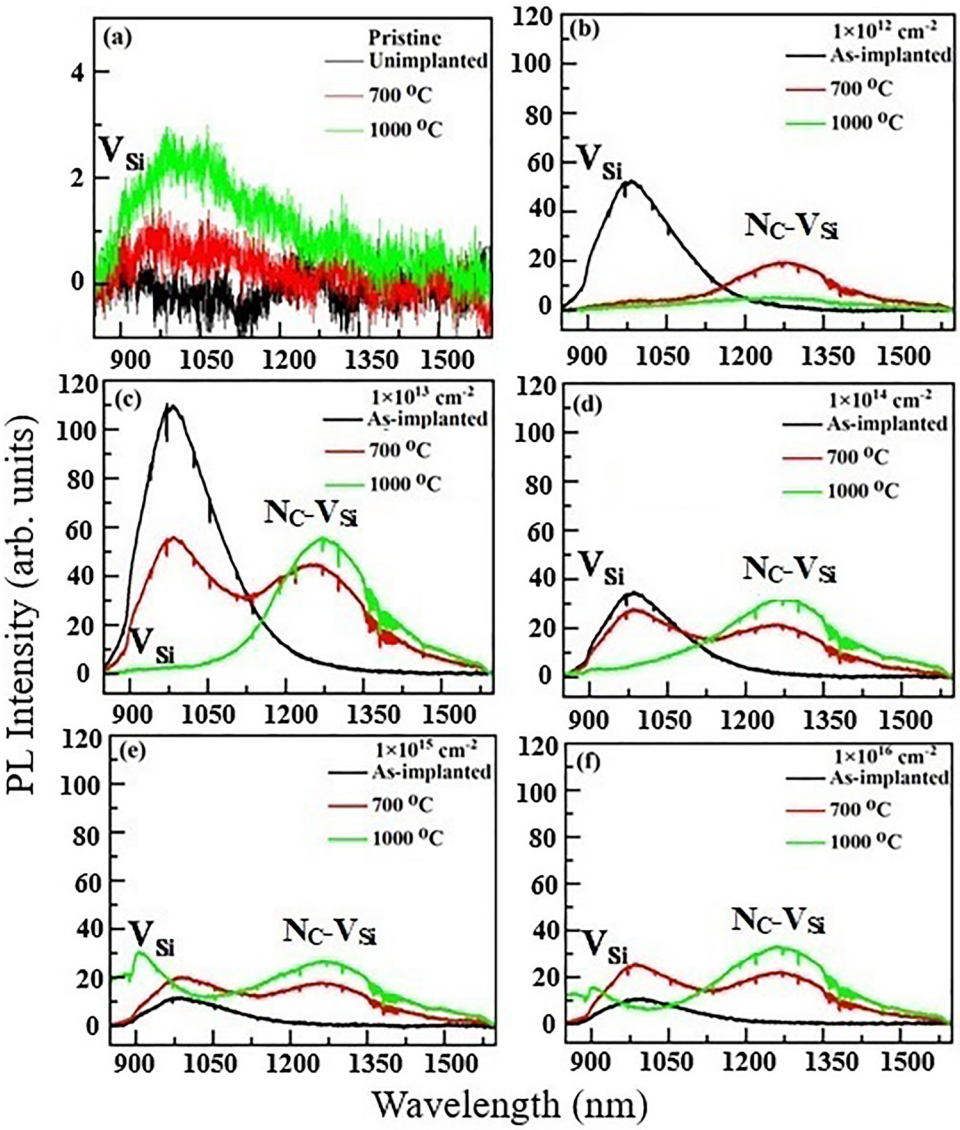

FIG. 7. Room temperature PL spectra of n-type 4H-SiC excited with 785 nm: (a) pristine and (b)–(f) as-implanted and after annealing at 700 and 1000 °C.

The N_C–V_{Si} center emission at around 1300 nm is absent in the irradiated samples for the range of fluences used and is activated after a thermal annealing of the irradiated wafers [Figs. 7(b)–7(f)].[14,21,32–36] The simultaneous decrease in the V_{Si} intensity and an increase of the N_C–V_{Si} center emission indicates the mitigation of V_{Si} in the lattice which combines with the nitrogen center already present in the pristine sample due to the n-type nature of wafer. This can be explained using two process: (1) mitigation: $N_C^+ + V_{Si}^- + e^- \rightarrow N_C V_{Si}^-$[38] and (b) multiple process: interstitial carbon (C_i) combines with N center and forms $(NC)_C$ which again combines with V_C–V_{Si} and produces N_C–V_{Si} centers. In addition, with a change in the annealing temperature from 700 to 1000 °C, the increase in the peak intensity with fluence shows the role of the post-implantation annealing in improving the concentration of the N_C–V_{Si} defect.

b. For an excitation wavelength 1064 nm. The N_C–V_{Si} center formation in n-type U200 wafers is also investigated using a 1064 nm excitation. The PL spectra shown in Figs. 8(a)–8(f) confirm that they are activated by post-implantation annealing as was shown using 785 nm (Fig. 7). The higher intensities using the 1064 nm excitation as compared to 785 nm is because of a more efficient activation due to its proximity to the N_C–V_{Si} center defect energy level. A similar behavior was observed for the V_{Si} emission (Ref. 34 and in the supplementary material). The PL spectra show that a fluence of 1×10^{13} cm^{-2} and an annealing temperature of 1000 °C result in the highest intensity of the N_C–V_{Si} center. Our results showing the creation of N_C–V_{Si} using low energy keV Si ions is promising from a practical aspect and suggests an advantage over proton irradiation in which unwanted intermediate complexes,

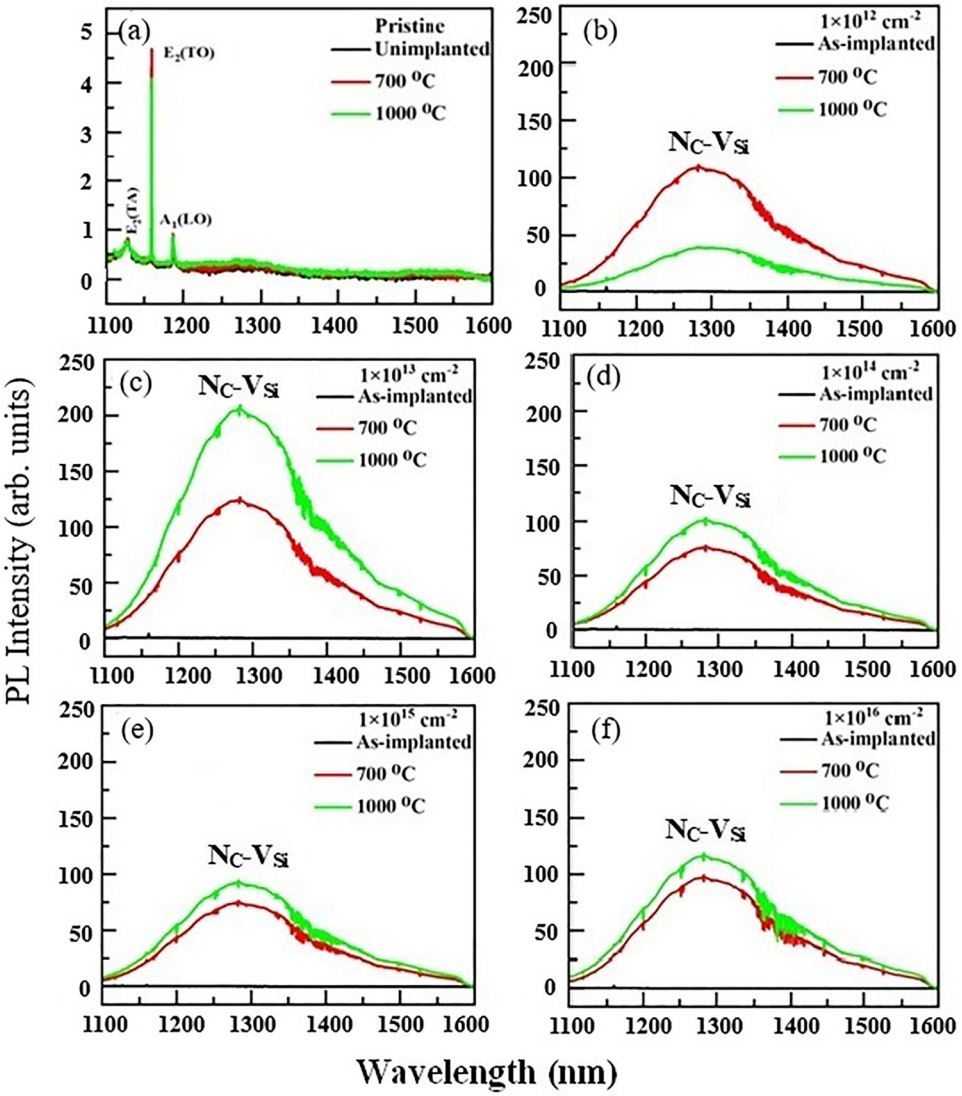

FIG. 8. Room temperature PL spectra of n-type U200 wafers excited at 1064 nm: (a) pristine and (b)–(f) as-implanted and after annealing at 700 and 1000 °C.

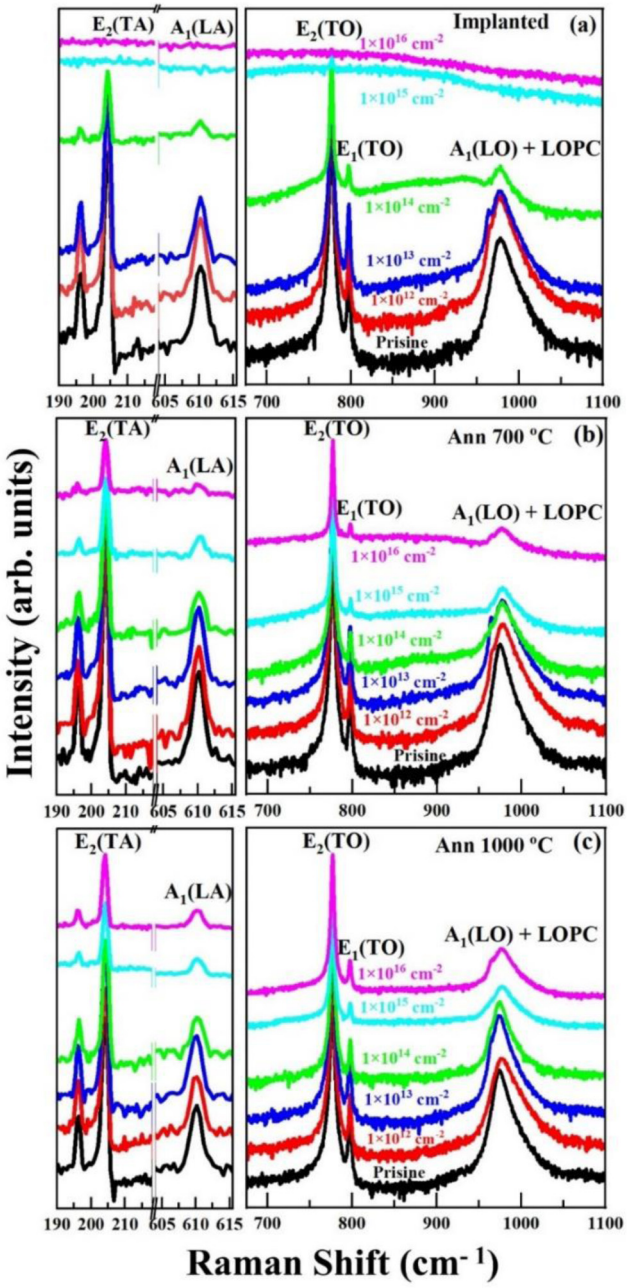

FIG. 9. First-order Raman spectra of n-type U200 wafers for (a) as-implanted, annealed at (b) 700 and (c) 1000 °C.

such as V_{Si}–H result in an inefficient conversion of V_{Si} into N_C–V_{Si}.[22,32–35] Further, the N_C–V_{Si} PL intensities using keV Si ions persist with sizeable intensities up to a high fluence of 1×10^{16} cm^{-2} after annealing, comparing well with the N_C–V_{Si} intensities obtained using 4 MeV Si ions[33] up to a fluence of 2×10^{14} cm^{-2}.

D. Raman spectra of ion-implanted and thermally annealed n-type U200 wafer

The Raman spectra of Si ion-implanted n-type U200 at various fluences is shown in Fig. 9(a) and those of the post-implanted thermally annealed at 700 and 1000 °C are depicted in Figs. 9(b) and 9(c), respectively.

The Raman spectra of the irradiated 4H-SiC up to a fluence of 1×10^{14} cm^{-2} remains the same as that of the pristine sample, with a decrease in the mode intensities. Thereafter, the features smear out at higher fluences of 1×10^{15} and 1×10^{16} cm^{-2}. This is because the ion-induced structural disorder leads to a breakdown of the translational symmetry and thereby induces an amorphization. An annealing at 700 °C leads to well-defined E_2 (TA), A_1 (LA), E_2 (TO), and A_1 (LO) modes at fluences of 1×10^{15} and 1×10^{16} cm^{-2} indicating a recovery of the damage and a recrystallization.[43] With a further increase in the annealing temperature to 1000 °C, the peak intensities are further enhanced indicating an improvement in the recrystallization [Figs. 9(b) and 9(c)]. The ion-induced crystalline to amorphous transitions and the recrystallization upon annealing are similar to previous high-resolution x-ray diffraction (HR-XRD), Raman spectroscopy, and Rutherford scattering spectroscopy studies.[43–46]

IV. CONCLUSION

The generation of the V_{Si} and N_C–V_{Si} centers in SiC using keV energies conveniently obtained from a modest implanter has been demonstrated. Their occurrence depends on the nitrogen-concentration as demonstrated though a comparison of n-type and semi-insulating HPSI wafers. The ion fluence and a post-implantation isochronal thermal annealing modulate the defect densities as observed though their PL signatures. The conversion of V_{Si} into N_c–V_{Si} with a variation of annealing temperature is also demonstrated. Low energy keV Si ions used in this study is promising from a practical aspect for creating N_C–V_{Si} and has advantages over the widely used proton irradiation of MeV energies. This work also demonstrates that N_C–V_{Si} persist with sizeable PL intensities up to a high fluence of 1×10^{16} cm^{-2} and compare well with earlier studies using MeV Si ions. Wavelength dependent photoluminescence spectroscopy gives further insights into the defects. The defect densities are correlated to the ion-induced structural disorder/amorphization and the thermally induced recrystallization investigated through Raman spectroscopy.

SUPPLEMENTARY MATERIAL

The supplementary material shows (i) the depth profiles of the silicon vacancies and implanted silicon referred to in paragraph 5 of Sec. I and (ii) a comparison of the photoluminescence intensities of the silicon vacancy using 532 and 785 nm lasers referred to in Sec. III C 1.

ACKNOWLEDGMENTS

Funding from DST-SERB (Grant No. CRG/2020/005455) and DST-JSPS Project (Nos. DST/INT/JSPS/P0326 and JPJSBP120217718) is acknowledged. G.G. thanks DST for the INSPIRE Fellowship (No. DST/AORC-IF/UPGRD/IF170870). S.R.

thanks Inter University Accelerator Centre for ion irradiation under BTR Proposal No. 67516.

AUTHOR DECLARATIONS

Conflict of Interest

The authors have no conflicts to disclose.

Author Contributions

Shyama Rath: Conceptualization (lead); Formal analysis (equal); Funding acquisition (lead); Investigation (equal); Methodology (equal); Project administration (lead); Resources (equal); Supervision (lead); Writing – original draft (equal); Writing – review & editing (equal). **Gaurav Gupta:** Data curation (equal); Formal analysis (equal); Investigation (equal); Methodology (equal); Writing – original draft (equal). **Shin-ichiro Sato:** Conceptualization (equal); Data curation (equal); Formal analysis (equal); Funding acquisition (supporting); Investigation (equal); Methodology (equal); Project administration (supporting); Resources (equal); Validation (equal); Writing – review & editing (equal).

DATA AVAILABILITY

The data that support the findings of this study are available from the corresponding author upon reasonable request.

REFERENCES

[1]S. E. Crawford, R. A. Shugayev, H. P. Paudel, P. Lu, M. Syamlal, P. R. Ohodnicki, B. Chorpening, R. Gentry, and Y. Duan, Adv. Quantum Technol. **4**, 2100048 (2021).
[2]G. Wolfowicz, F. J. Heremans, C. P. Anderson, S. Kanai, H. Seo, A. Gali, G. Galli, and D. D. Awschalom, Nat. Rev. Mater. **6**, 906 (2021).
[3]F. J. Heremans, C. G. Yale, and D. D. Awschalom, Proc. IEEE **104**, 2009 (2016).
[4]M. Ruf, N. H. Wan, H. Choi, D. Englund, and R. Hanson, J. Appl. Phys. **130**, 070901 (2021).
[5]S. Hong, M. S. Grinolds, L. M. Pham, D. Le Sage, L. Luan, R. L. Walsworth, and A. Yacoby, MRS Bull. **38**, 155 (2013).
[6]L. Childress and R. Hanson, MRS Bull. **38**, 134 (2013).
[7]L. Gordon, A. Janotti, and C. G. Van de Walle, Phys. Rev. B **92**, 045208 (2015).
[8]T. Kobayashi, K. Harada, Y. Kumagai, F. Oba, and Y. Matsushita, J. Appl. Phys. **125**, 125701 (2019).
[9]E. Janzén, A. Gali, P. Carlsson, A. Gällström, B. Magnusson, and N. T. Son, Physica B **404**, 4354 (2009).
[10]P. G. Baranov, A. P. Bundakova, A. A. Soltamova, S. B. Orlinskii, I. V. Borovykh, R. Zondervan, R. Verberk, and J. Schmidt, Phys. Rev. B **83**, 125203 (2011).
[11]M. Widmann, S. Y. Lee, T. Rendler, N. T. Son, H. Fedder, S. Paik, L. P. Yang, N. Zhao, S. Yang, I. Booker, A. Denisenko, M. Jamali, S. A. Momenzadeh, I. Gerhardt, T. Ohshima, A. Gali, E. Janzén, and J. Wrachtrup, Nat. Mater. **14**, 164 (2015).
[12]D. Riedel, F. Fuchs, H. Kraus, S. Väth, A. Sperlich, V. Dyakonov, A. A. Soltamova, P. G. Baranov, V. A. Ilyin, and G. V. Astakhov, Phys. Rev. Lett. **109**, 226402 (2012).
[13]D. J. Christle, A. L. Falk, P. Andrich, P. V. Klimov, J. U. Hassan, N. T. Son, E. Janzén, T. Ohshima, and D. D. Awschalom, Nat. Mater. **14**, 160 (2015).
[14]V. Ivády, J. Davidsson, N. T. Son, T. Ohshima, I. A. Abrikosov, and A. Gali, Phys. Rev. B **96**, 161114 (2017).
[15]M. E. Bathen, A. Galeckas, J. Müting, H. M. Ayedh, U. Grossner, J. Coutinho, Y. K. Frodason, and L. Vines, npj Quantum Inf. **5**, 111 (2019).
[16]J. W. Steeds, Phys. Rev. B **80**, 245202 (2009).
[17]S. Castelletto, B. C. Johnson, V. Ivády, N. Stavrias, T. Umeda, A. Gali, and T. Ohshima, Nat. Mater. **13**, 151 (2014).
[18]N. T. Son, P. Carlsson, J. ul Hassan, E. Janzén, T. Umeda, J. Isoya, A. Gali, M. Bockstedte, N. Morishita, T. Ohshima, and H. Itoh, Phys. Rev. Lett. **96**, 055501 (2006).
[19]L. Torpo, T. E. M. Staab, and R. M. Nieminen, Phys. Rev. B **65**, 085202 (2002).
[20]U. Gerstmann, E. Rauls, T. Frauenheim, and H. Overhof, Phys. Rev. B **67**, 205202 (2003).
[21]H. J. von Bardeleben, J. L. Cantin, E. Rauls, E. Rauls, and U. Gerstmann, Phys. Rev. B **92**, 064104 (2015).
[22]S. A. Zargaleh, B. Eble, S. Hameau, J. L. Cantin, L. Legrand, M. Bernard, F. Margaillan, J. S. Lauret, J. F. Roch, H. J. von Bardeleben, E. Rauls, U. Gerstmann, and F. Treussart, Phys. Rev. B **94**, 060102 (2016).
[23]Y. Zhu, B. Kovos, M. Onizhuk, D. Awschalom, and G. Galli, Phys. Rev. Mater. **5**, 074602 (2021).
[24]K. Khazen and H. J. Von Bardeleben, Front. Quantum Sci. Technol. **2**, 1115039 (2023).
[25]R. Maboudian, C. Carraro, D. G. Senesky, and C. S. Roper, J. Vac. Sci. Technol. A **31**, 50805 (2013).
[26]A. M. Smith, M. C. Mancini, and S. Nie, Nat. Nanotechnol. **4**, 710 (2009).
[27]E. Sörman, N. T. Son, W. M. Chen, O. Kordina, C. Hallin, and E. Janzén, Phys. Rev. B **61**, 2613 (2000).
[28]G. Alfieri, E. V. Monakhov, B. G. Svensson, and A. Hallén, J. Appl. Phys. **98**, 113524 (2005).
[29]N. T. Son and I. G. Ivanov, J. Appl. Phys. **129**, 215702 (2021).
[30]S. B. Orlinski, J. Schmidt, E. N. Mokhov, and P. G. Baranov, Phys. Rev. B **67**, 125207 (2003).
[31]F. Fuchs, B. Stender, M. Trupke, D. Simin, J. Pflaum, V. Dyakonov, and G. V. Astakhov, Nat. Commun. **6**, 7578 (2015).
[32]M. Rühl, C. Ott, S. Götzinger, M. Krieger, and H. B. Weber, Appl. Phys. Lett. **113**, 1 (2018).
[33]S. I. Sato, T. Narahara, Y. Abe, Y. Hijikata, T. Umeda, and T. Ohshima, J. Appl. Phys. **126**, 083105 (2019).
[34]M. E. Bathen, A. Galeckas, J. Coutinho, and L. Vines, J. Appl. Phys. **127**, 085701 (2020).
[35]T. Narahara, S. Sato, K. Kojima, Y. Hijikata, and T. Ohshima, Appl. Phys. Express **14**, 021004 (2021).
[36]J. Wang, X. Zhang, Y. Zhou, K. Li, Z. Wang, P. Peddibhotla, F. Liu, S. Bauerdick, A. Rudzinski, Z. Liu, and W. Gao, ACS Photonics **4**, 1054 (2017).
[37]J. F. Wang, Q. Li, F. F. Yan, H. Liu, G. P. Guo, W. P. Zhang, X. Zhou, L. P. Guo, Z. H. Lin, J. M. Cui, X. Y. Xu, J. S. Xu, C. F. Li, and G. C. Guo, ACS Photonics **6**, 1736 (2019).
[38]T. Brodar, L. Bakrač, I. Capan, T. Ohshima, L. Snoj, V. Radulović, and Ž Pastuović, Crystals **10**, 845 (2020).
[39]S. Nakashima and H. Harima, Phys. Status Solidi A **162**, 39 (1997).
[40]J. C. Burton, L. Sun, M. Pophristic, S. J. Lukacs, F. H. Long, Z. C. Feng, and I. T. Ferguson, J. Appl. Phys. **84**, 6268 (1998).
[41]J. C. Burton, L. Sun, F. H. Long, Z. C. Feng, and I. T. Ferguson, Phys. Rev. B **59**, 7282 (1999).
[42]M. Shu, S. Sati, S. Seiichi, S. Y. Masuyama, Y. Yamazaki, T. Ohshima, K. Murata, H. Tsuchida, and Y. Hijikata, J. Appl. Phys. **133**, 154402 (2023).
[43]G. Gupta, P. Jozwik, S. Ojha, G. R. Umapathy, A. Pandey, and S. Rath, Appl. Surf. Sci. **665**, 160296 (2024).
[44]T. C. Hain, F. Fuchs, V. A. Soltamov, P. G. Baranov, G. V. Astakhov, H. T. Hertel, and V. Dyakonov, J. Appl. Phys. **115**, 1508 (2014).
[45]S. Sorieul, J. M. Costantini, L. Gosmain, L. Thomé, and J. J. Grob, J. Phys.: Cond. Matt. **18**, 5235 (2006).
[46]A. Chakravorty, B. Singh, H. Jatav, S. Ojha, J. Singh, D. Kanjilal, and D. Kabiraj, J. Appl. Phys. **128**, 165901 (2020).